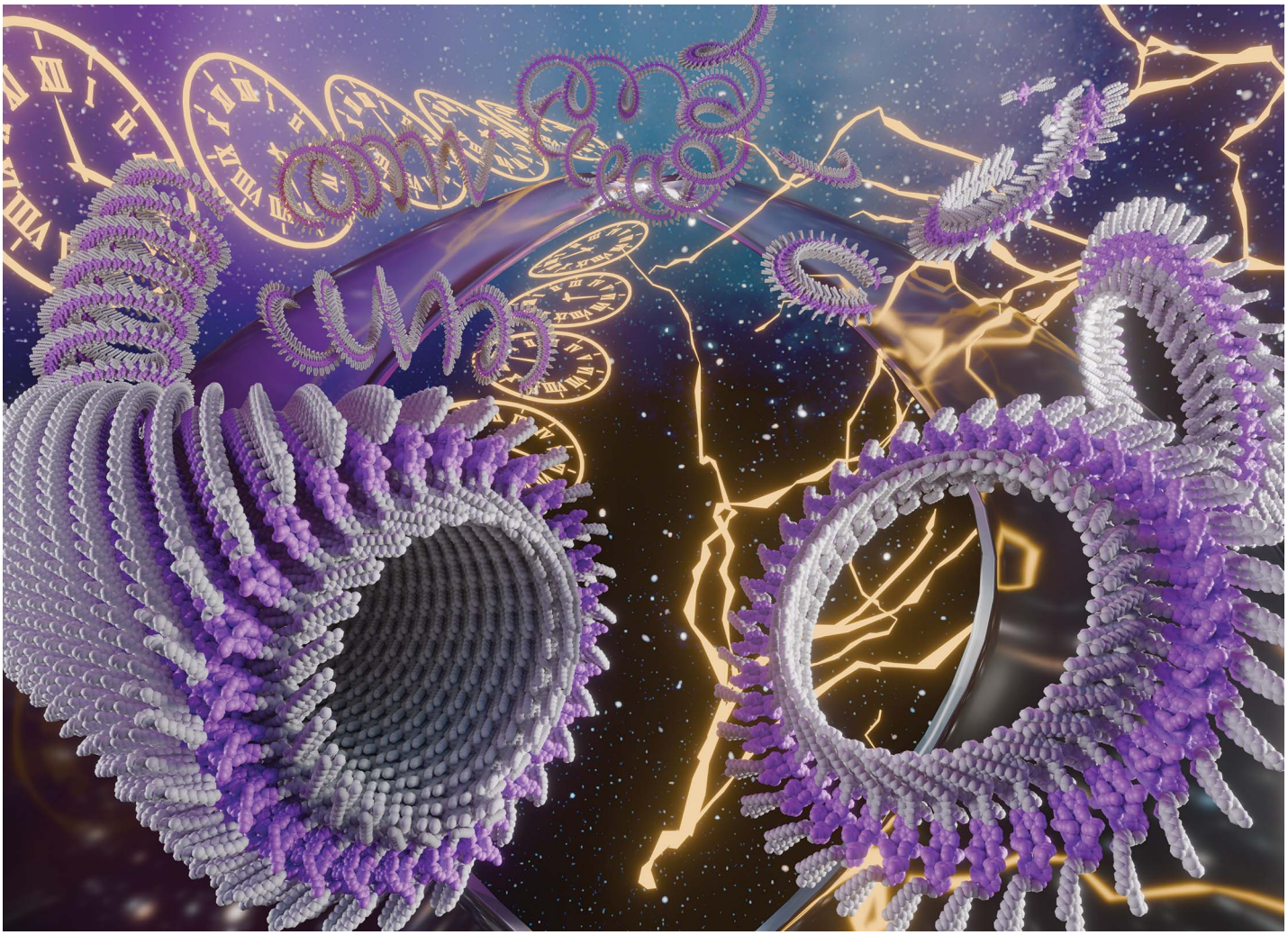

Showcasing research from Professor Yagai's laboratory, Institute for Advanced Academic Research, Chiba University, Japan.

Curvature-emergent supramolecular polymerization of a porphyrin dyad with a scissor-shaped motif

Curvature-emergent supramolecular polymerization of a scissor-shaped porphyrin dyad is depicted as a time-evolving bifurcation in which helicoidal assemblies diverge into tubular superstructures or, upon sonication, into rings.

Image reproduced by permission of Ryuichi Kawai and Shiki Yagai from *Chem. Sci.*, 2026, **17**, 2559.

As featured in:

See Shiki Yagai *et al.*, *Chem. Sci.*, 2026, **17**, 2559.

ROYAL SOCIETY OF CHEMISTRY

rsc.li/chemical-science

Registered charity number: 207890

Chemical Science

ROYAL SOCIETY OF CHEMISTRY

EDGE ARTICLE

View Article Online
View Journal | View Issue

Cite this: *Chem. Sci.*, 2026, **17**, 2559

All publication charges for this article have been paid for by the Royal Society of Chemistry

Received 8th December 2025
Accepted 14th January 2026

DOI: 10.1039/d5sc09619g

rsc.li/chemical-science

Curvature-emergent supramolecular polymerization of a porphyrin dyad with a scissor-shaped motif

Ryuichi Kawai,[a] Soichiro Ogi,[b] Hiroki Hanayama,[c] Ryo Kudo[a] and Shiki Yagai *[cd]

Curvature has recently emerged as a key structural parameter that dictates the pathway and topology of supramolecular polymerization. We previously showed that scissor-shaped azobenzene dyads, dimerized through a xylylene spacer bearing long alkyl chains, undergo folding-induced self-assembly to yield curvature-derived architectures such as nanorings and nanotubes. Here we extend this scaffold to a bulkier chromophore and demonstrate that the curvature-directed pathway is preserved. Dimerization of tetraphenylporphyrin on the scissor-shaped backbone yields a molecule that, in nonpolar solvents, exhibits a split, bathochromically shifted Soret band. This finding suggests intra- and intermolecular J-type exciton coupling during folding-induced supramolecular polymerization. AFM revealed the formation of helically coiled supramolecular polymers (helicoids). These helicoids evolve into nanotubes over time; applying sonication beforehand induces fragmentation that closes the curved segments into discrete toroids.

Introduction

Supramolecular polymers formed through noncovalent interactions have been extensively studied owing to their dynamic nature derived from reversible bonding, as well as their unique optical and electronic properties.[1,2] Among them, supramolecular polymers that deviate from one-dimensional structures—such as helical coils (helicoids) and toroidal architectures—exhibit structural diversity and dynamic characteristics reminiscent of protein assemblies.[3–5] Although a few supramolecular systems forming helicoids or toroids have been reported,[6] they have not been understood in terms of curved supramolecular polymerization.[7,8] We believe that explicitly introducing the concept of curvature into supramolecular polymerization represents a fundamental strategy for creating curved architectures. In curvature-guided supramolecular polymerization, toroidal structures generally emerge as kinetic products, whereas helicoidal structures correspond to the thermodynamic products.[7] Only a limited number of molecular systems exhibit such behavior, among which barbiturate-based π-conjugated systems developed by our group are representative examples.[7,8]

We have demonstrated that barbiturate-functionalized π-conjugated molecules inherently yield curvature upon self-assembly, forming diverse curved morphologies depending on the assembly conditions. For instance, under thermodynamic conditions such as slow cooling from a hot monomer solution, open-ended polymerization accompanied by curvature is favored, yielding helicoidal structures.[4,7] In contrast, under kinetic conditions such as rapid cooling, ring-closing polymerization predominates, leading to toroidal structures.[9,10] To generalize this curvature-dependent mechanism that governs open- and closed-ring topologies, it is essential to verify its universality using a distinct molecular scaffold that also exhibits curvature-induced supramolecular polymerization.

As another platform for curvature-driven supramolecular polymerization, we focused on scissor-shaped azobenzene dyads,[11] in which two azobenzene units are dimerized through a 3,4,5-tris(dodecyloxy)-xylylene spacer.[12,13] In nonpolar solvents, the dyad adopts a wedge-shaped folded conformation stabilized by intramolecular hydrogen bonding and π–π interactions, and the intermolecular association of these folded dyads gives rise to toroids.[14–16] Thus, the azobenzene dyad forms curved ring-like architectures through wedge-shaped folding; however, it did not exhibit an open-ended pathway toward helicoidal structures, as observed for the barbiturate derivatives.

In this study, we explored the possibility of realizing an open-ended pathway by introducing a chromophore with stronger aggregation propensity than azobenzene into the scissor-

[a]*Division of Advanced Science and Engineering, Graduate School of Engineering, Chiba University, 1-33 Yayoi-cho, Inage-ku, Chiba 263-8522, Japan*

[b]*Integrated Research Consortium on Chemical Science (IRCCS), Nagoya University Furo, Chikusa, Nagoya 464-8682, Japan*

[c]*Department of Applied Chemistry and Biotechnology, Graduate School of Engineering, Chiba University, 1-33 Yayoi-cho, Inage-ku, Chiba 263-8522, Japan. E-mail: yagai@faculty.chiba-u.jp*

[d]*Institute for Advanced Academic Research (IAAR), Chiba University, 1-33 Yayoi-cho, Inage-ku, Chiba 263-8522, Japan*

shaped scaffold, thereby testing whether the scissor-shaped motif can act as a universal curvature-inducing unit independent of the chromophore. To this end, we designed and synthesized the scissor-shaped porphyrin dyad **1**. Porphyrins, with their strong intermolecular interactions and pronounced spectroscopic sensitivity to aggregation, have long served as functional cores in supramolecular assemblies.[17–20] Examination of the self-assembly behavior of **1** in nonpolar solvents revealed that the molecules initially form amorphous kinetic aggregates, which subsequently evolve into helicoidal supramolecular polymers exhibiting a split Soret-band characteristic of J-type aggregates. These helicoids spontaneously transformed into nanotubes. Although toroids could not be obtained directly from the amorphous state under kinetic conditions, sonication of the helicoids enabled their transformation into toroids. Taken together, these results demonstrate that the scissor-shaped scaffold can drive curvature-directed self-assembly not only of azobenzene but also of porphyrin chromophores, thereby functioning as a universal curvature-inducing unit for supramolecular polymerization.

Result and discussion

Porphyrin dyad **1** was synthesized and characterized by ^{1}H and ^{13}C NMR spectroscopies as well as mass spectrometry (Scheme S1). The self-assembly of **1** in methylcyclohexane (MCH, $c = 50$ μM) was investigated by variable-temperature UV/Vis absorption spectroscopy. At 100 °C, **1** displayed Soret- and Q-bands at 418 and 551/593 nm, respectively (Fig. 2a, red line). Under identical conditions, the reference monad **2** (Scheme S1) showed slightly shifted maxima at 420 and 549/589 nm (Fig. S1). Notably, **1** exhibited a substantially broader Soret-band with full width at half maximum (FWHM = 1275 cm^{-1}) compared to that of **2** (FWHM = 657 cm^{-1}). This pronounced broadening suggests the presence of intramolecular electronic interactions between the two porphyrin chromophores in **1**. Taken together, these observations indicate that **1** adopts an intramolecularly folded conformation in MCH at 100 °C (Fig. 1a).

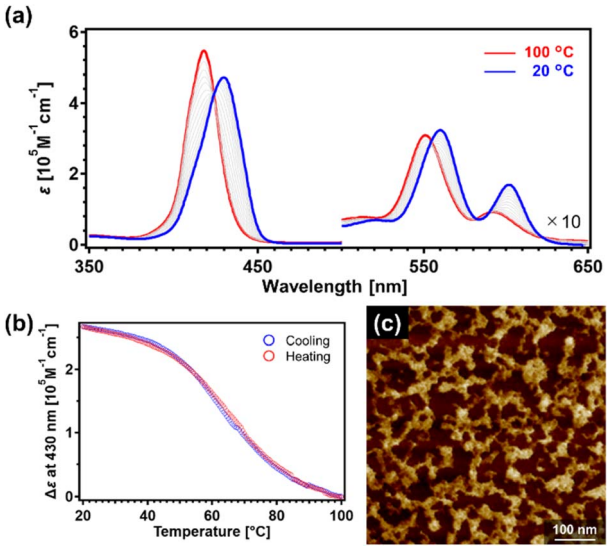

Fig. 2 (a) UV/Vis absorption spectra of **1** in MCH ($c = 50$ μM) upon cooling from 100 °C (red line) to 20 °C (blue line) at a rate of 1 °C min^{-1}. The intermediate spectra were measured every 5 °C. (b) Cooling (blue plots) and heating (red plots) profiles obtained by plotting the change in absorption at 430 nm as a function of temperature. (c) AFM image of an **Amo** film prepared by spin-coating an MCH solution of **1** immediately after cooling from 100 °C to 20 °C at a rate of 1 °C min^{-1}.

Upon cooling the hot monomeric solution to 20 °C at a rate of 1 °C min^{-1}, the Soret- and Q-band maxima bathochromically shifted to 430 and 560/602 nm (Fig. 2a, blue line), respectively, indicating J-type stacking of the porphyrin chromophores.[21] Monitoring the growth of the absorbance at 430 nm during cooling revealed a sigmoidal aggregation curve, which was found to depend on concentration, indicating the isodesmic supramolecular polymerization mechanism through

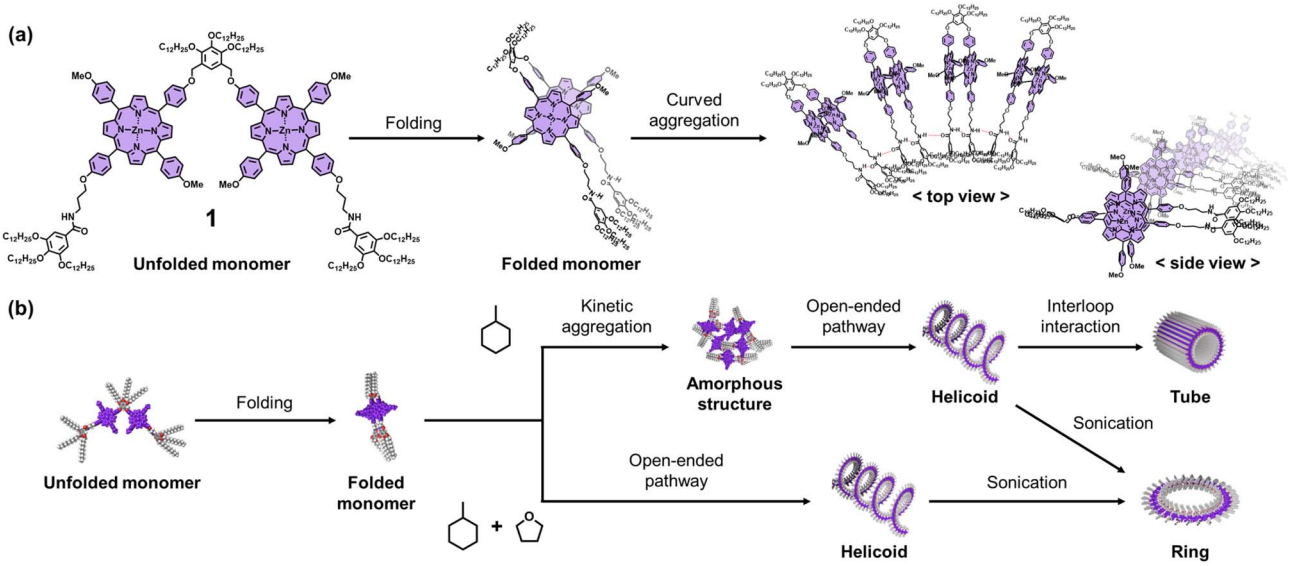

Fig. 1 (a) Molecular structure of **1**. (b) schematic representation of its self-assembly process to form helicoid, tube and ring.

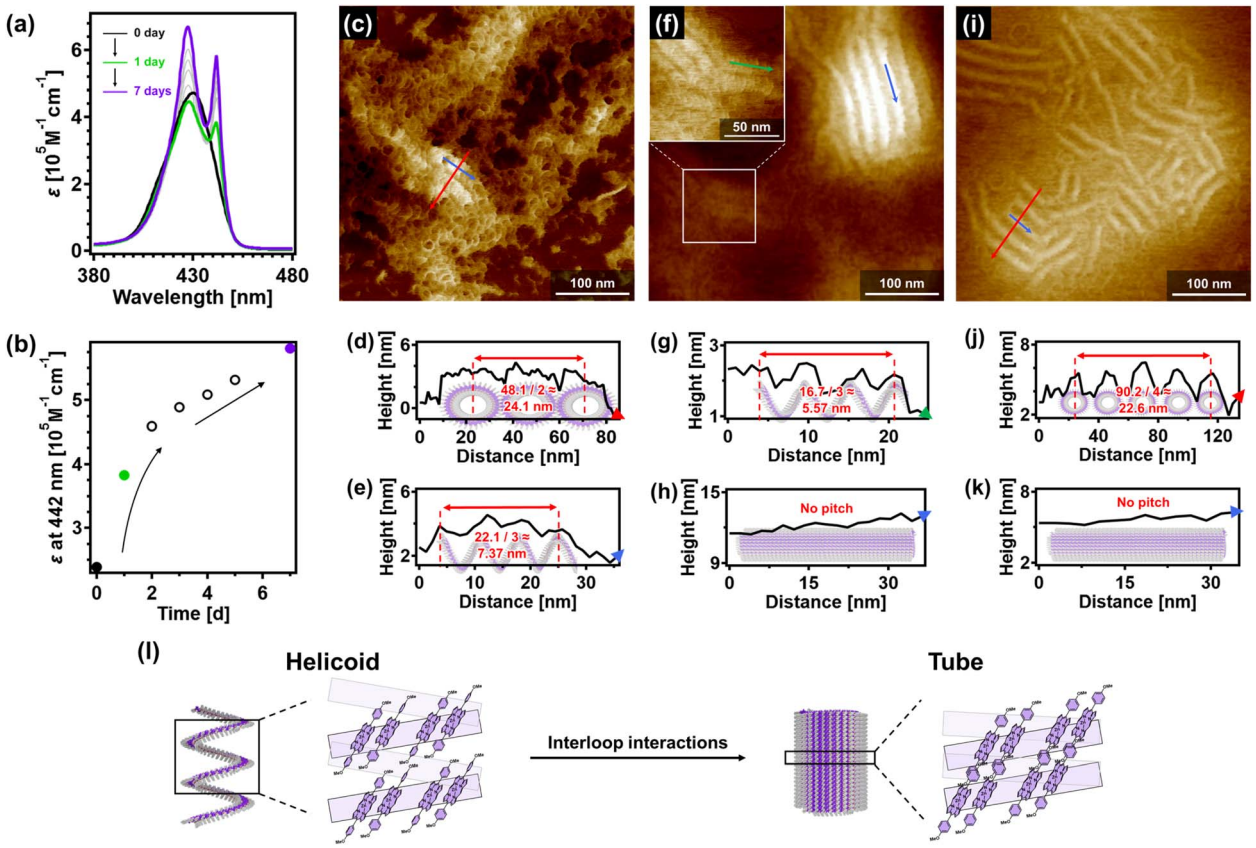

Fig. 3 (a) UV/Vis absorption spectra of **1** ($c = 50$ μM) in MCH aged from 0 day (black line) to 1 day (green line) and 7 days (purple line), respectively. (b) Time-dependent change in the molar extinction coefficient at 442 nm during the transition from **Amo** to SP_{tube}. (c) AFM image of assemblies of **1** aged for 1 day. (d and e) AFM cross-sectional analysis of SP_{hel} along the (d) red and (e) blue arrows in (c), respectively. (f and i) AFM images of assemblies of **1** obtained after aging for (f) 3 days and (i) 7 days, respectively. (g and h) AFM cross-sectional analysis of SP_{hel} and SP_{tube} along the (g) green and (h) blue arrows in (f), respectively. (j and k) AFM cross-sectional analysis of SP_{tube} along the (j) red and (k) blue arrows in (i), respectively. (l) Schematic illustration of the transformation from SP_{hel} to SP_{tube}.

intermolecular interactions (Fig. 2b and S2).[22,23] Because subsequent heating of the solution did not show thermal hysteresis, the thermodynamic parameters were obtained by global fitting of the heating curves using an isodesmic model. The analysis provided the standard enthalpy ($\Delta H°$) and entropy ($\Delta S°$) of −115 kJ mol^{-1} and −263 J mol^{-1} K^{-1}, respectively. Compared with the reference monad **2** (Fig. S3), the larger enthalpic gain and the more pronounced entropic loss can be attributed to intramolecular folding, which preorganizes the molecular conformation, strengthens intermolecular interactions, and thereby enhances the overall thermodynamic stability of the assemblies. Atomic force microscopy (AFM) imaging of the assemblies of **1** displayed only ill-defined amorphous structures (**Amo**, Fig. 2c). In the FT-IR measurements, N–H stretching vibration bands of the amide group were observed at 3415/3317 cm^{-1} in MCH, shifted from 3449 cm^{-1} in $CHCl_3$, in which the molecules are molecularly dissolved as monomers (Fig. S4). Furthermore, the C=O stretching vibration bands of the amide group were not clearly observed in MCH.[24] This result suggested that the amide group of **1** did not form well-defined hydrogen bonding in **Amo**.

Aging of the **Amo** solution at 20 °C for 1 day caused the Soret maximum to split into two bands at 428 and 442 nm (Fig. 3a and b; black to green data). AFM imaging of this solution revealed that **1** self-assembled into helicoidal structures (**SP_{hel}**, Fig. 3c).[4,25] AFM cross-sectional analysis showed that the apparent diameter of **SP_{hel}**, observed in a flattened state after drying, was approximately 24 nm, and the helical pitch was about 7.4 nm (Fig. 3d and e). The splitting of the Soret-band upon aging is likely attributable to intramolecular stacking between the two porphyrin chromophores within the dyad, in conjunction with intermolecular stacking that drive supramolecular polymerization. Notably, the corresponding free-base porphyrin dyad also undergoes intramolecular folding and forms helically twisted fibers, yet it does not develop any detectable curved architectures such as helicoids or tubes (Fig. S5).[26] This contrast indicates that folding alone is not sufficient to induce curvature. Rather, Zn-metalation strengthens the intramolecular stacking and locks the folded conformer into a more wedge-like geometry, introducing an inherent structural bias that predisposes the aggregates toward curved structures.

Interestingly, further aging of the **SP_{hel}** solution for several more days led to an increase in the molar extinction coefficient (ε) of the two absorption bands, accompanied by sharpening. The time-dependent change in ε at 442 nm upon aging from

Amo revealed a first-order increase corresponding to the formation of $\mathbf{SP_{hel}}$ within the first 2 days, followed by a zero-order regime (Fig. 3b). This second phase change persisted even after 7 days of aging from **Amo**. AFM imaging of the 3-day-aged solution showed an indistinct helical pitch, and when observable, the pitch narrowed to approximately 5.6 nm (Fig. 3f–h). After 7 days of aging, the helical pitch was no longer discernible, whereas the diameter remained essentially unchanged at approximately 23 nm in the AFM images (Fig. 3i–k). These observations indicate that $\mathbf{SP_{hel}}$ spontaneously transformed into tubular structures[3,27–31] ($\mathbf{SP_{tube}}$) over time through helical interloop interactions (non-neighboring contacts).[32–34] The sharpening of the absorption bands accompanying this structural transition can be thus attributed to more homogeneous excitonic interactions,[35,36] arising not only from neighboring but also from non-neighboring chromophore interactions within the $\mathbf{SP_{hel}}$ backbone (Fig. 3l). To probe non-neighboring interactions, $\mathbf{SP_{hel}}$ was prepared and aged in MCH containing 20% (v/v) toluene, a solvent with high affinity for aromatic units. Under these conditions, no structural transition was observed even after 20 days (Fig. S6). Furthermore, in the UV/Vis spectra, the absorption maximum at 264 nm of benzene units hypsochromically shifted to 260 nm upon aging for 1 day ($\mathbf{SP_{hel}}$) to 7 days ($\mathbf{SP_{tube}}$), indicating weak interactions between the phenyl groups (Fig. S7). Taken together, this finding strongly suggests that the structural evolution of $\mathbf{SP_{hel}}$ is driven by non-neighboring interactions among the phenyl groups at the *meso* positions of the porphyrin (Fig. 3l).

Although dyad **1** exhibited a gradual self-assembly pathway from **Amo** to $\mathbf{SP_{hel}}$ and subsequently to $\mathbf{SP_{tube}}$, the kinetics of supramolecular polymerization from **Amo** to $\mathbf{SP_{hel}}$ displayed considerable variability, with the required time ranging from 1 day to 1 month. In some cases, the structural transition was not observed at all. Notably, the transition time exhibited seasonal dependence, proceeding faster in summer but slower in winter. This phenomenon can be attributed to trace amounts of water in MCH, which influence the self-assembly process, as previously reported by Meijer and coworkers.[37,38] According to this report, trace water could induce destabilization of **Amo**. Consistently, upon varying the water content in MCH, the required time for the structural transition decreased with increasing water concentration (Fig. S8). However, further investigation of the water effect was hampered by its limited solubility in MCH. To address this, we employed THF, which is highly miscible with MCH, to promote destabilization of **Amo** through interaction with the zinc porphyrin or the amide group of **1**. The UV/Vis spectrum of **1** ($c = 54$ μM) in MCH containing 0.7% (v/v) THF (1760 eq. relative to **1**) at 100 °C displayed a Soret-band at 422 nm (Fig. 4a, red line), shifted by 4 nm compared to that in pure MCH at 100 °C, indicating coordination of THF to the zinc porphyrin. Upon cooling this solution to 0 °C at a rate of 1 °C $\mathrm{min^{-1}}$, the Soret-band underwent a bathochromic shift and split into two distinct J-bands with maxima at 423 and 442 nm, respectively (Fig. 4a, blue line). AFM imaging of this solution revealed that **1** self-assembled into $\mathbf{SP_{hel}}$ with the same diameter and helical pitch as those observed in pure MCH (Fig. 4c–e).

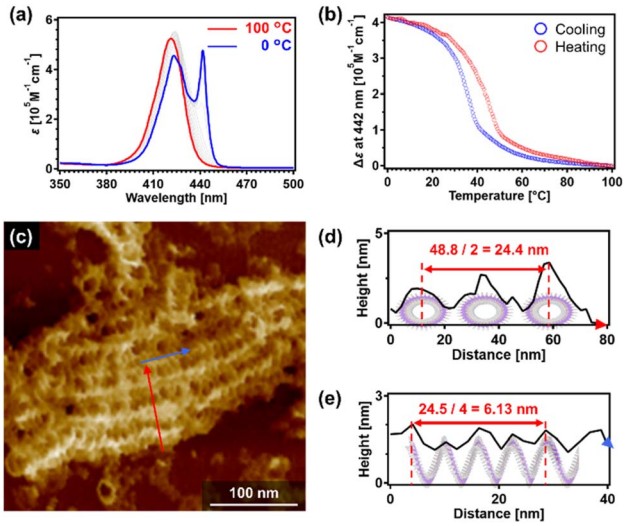

Fig. 4 (a) UV/Vis absorption spectra of **1** in MCH including 0.7% (v/v) of THF ($c = 54$ μM) upon cooling from 100 °C (red line) to 0 °C (blue line) at a rate of 1 °C $\mathrm{min^{-1}}$. The intermediate spectra were measured every 5 °C. (b) Cooling (blue plots) and heating (red plots) profiles obtained by plotting the change in absorption at 442 nm as a function of temperature. (c) AFM image of the resulting assemblies. (d and e) AFM cross-sectional analyses along the (d) red and (e) blue arrows in (c), respectively.

To gain mechanistic insight into the helicoidal supramolecular polymerization mechanism of $\mathbf{SP_{hel}}$ in mixed MCH/THF solvent, we monitored the temperature-dependent growth of the Soret-band absorbance at 442 nm (Fig. 4b). Between 100 and 39 °C, the absorbance change followed a sigmoidal profile, suggesting the formation of **Amo** as an intermediate state.[24] In contrast, from 39 to 0 °C, a non-sigmoidal profile was observed, indicative of a cooperative supramolecular polymerization mechanism.[23,32] Upon heating, an onset temperature appeared at 50 °C with pronounced thermal hysteresis, which was found to depend on concentration. Assuming **Amo** as the precursor state of $\mathbf{SP_{hel}}$, heating traces recorded at various concentrations were fitted at the lower onset temperature using the cooperative model, and the thermodynamic parameters were extracted by a modified van't Hoff analysis.[39] This yielded $\Delta H^\circ = -133$ kJ $\mathrm{mol^{-1}}$ and $\Delta S^\circ = -326$ J $\mathrm{mol^{-1}\ K^{-1}}$ (Fig. S9). Despite the simplified assumption in the van't Hoff analysis for $\mathbf{SP_{hel}}$ formation that the monomer concentration at the onset temperature corresponds to the total monomer concentration, and despite the presence of THF, which suppresses supramolecular polymerization, $\mathbf{SP_{hel}}$ still exhibited a larger enthalpic gain and a greater entropic loss than **Amo**. These results indicate that $\mathbf{SP_{hel}}$ adopts a more highly ordered molecular packing.

Based on these results, we believe that THF accelerates the transition from **Amo** to $\mathbf{SP_{hel}}$ by destabilizing **Amo**. Coordination of THF to the central zinc shifts the equilibrium between the monomer and **Amo** toward the monomeric state, which subsequently undergoes nucleation and elongation to form $\mathbf{SP_{hel}}$. To verify that THF does not significantly influence the intra- and intermolecular interactions between porphyrin units, THF was added to solutions of **Amo** and $\mathbf{SP_{hel}}$. In the UV/Vis

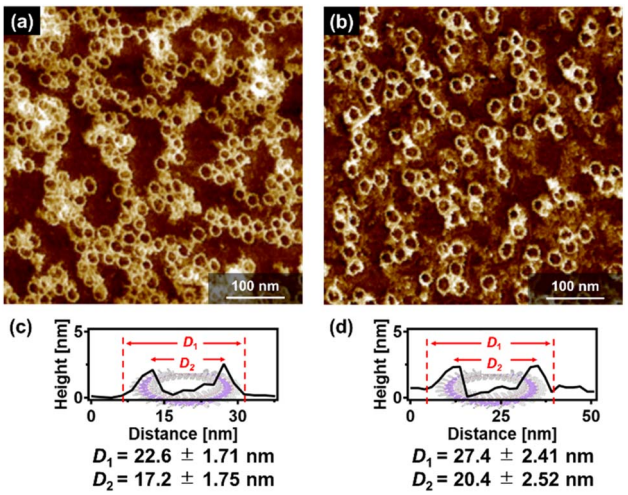

Fig. 5 (a and b) AFM images of SP_{ring} obtained by sonicating a SP_{hel} solution of **1** (c = 50 μM) in (a) MCH and (b) MCH including 0.7% (v/v) THF. (c and d) AFM cross-sectional analyses of representative SP_{ring} structures in (a) and (b), respectively. Average outer diameters (D_1) and top-to-top diameters (D_2) were determined from 100 SP_{ring} structures.

absorption spectra, the **Amo** solution showed a minor change whereas the SP_{hel} solution remained unchanged (Fig. S10). Therefore, we conclude that the role of THF is not to enhance the intra- and intermolecular interactions between the porphyrin units, but rather to facilitate the initiation of supramolecular polymerization by destabilizing **Amo**.

In our platform of barbiturate-based curved supramolecular polymerization,[7] the assembly pathway is programmable by cooling rate applied for molecularly dissolved solution at high temperature. Rapid cooling (quenching) biases the ring-closing route to toroids (kinetically trapped), whereas slow cooling preserves the rotational sense and promotes interloop contacts, yielding helicoids as the thermodynamic product. This cooling-rate dependence—kinetic rings *versus* thermodynamic helicoids—is a general feature of our barbiturate systems with curvature-emergent stacking. However, rings were not obtained upon quenching of **1**, since this molecule preferentially forms **Amo** under kinetic control, followed by the supramolecular polymerization into SP_{hel}. This outcome prompted us to pursue a top-down transformation of SP_{hel} into toroidal species by sonication.

Upon sonication of SP_{hel} in both pure MCH and mixed MCH/THF solvents for 15 min, dynamic light scattering (DLS) measurements revealed a pronounced reduction in hydrodynamic diameter for both systems (Fig. S11). Subsequent AFM imaging showed an almost quantitative conversion into discrete ring structures (SP_{ring}, Fig. 5a and b).[40–47] AFM cross-sectional analysis indicated that the outer diameters of SP_{ring} closely matched those of the parent SP_{hel} assemblies (Fig. 5c and d), suggesting that SP_{hel} was fragmented while retaining its curvature, implying that the helicoidal structures underwent fragmentation while largely preserving their intrinsic curvature, followed by spontaneous ring closure. In line with this interpretation, the UV/Vis absorption spectra displayed only a small change in the Soret-band after sonication (Fig. S12), indicating that the chromophoric packing remained essentially unperturbed. These observations demonstrate that the scissor-shaped molecular design retains a strong propensity for curvature-directed assembly, enabling the system to reorganize into kinetically favored toroidal structures even when constructed from highly aggregative chromophores such as porphyrins.

In contrast, sonication of SP_{tube} did not lead to a measurable reduction in hydrodynamic diameter, and AFM imaging confirmed that the tubular assemblies remained intact (Fig. S13). This striking difference in mechanical response highlights the strong influence of interloop interactions:[30] their presence in SP_{tube} confers pronounced mechanical stability, whereas their absence in SP_{hel} renders the assemblies susceptible to curvature-preserving fragmentation. Thus, even at the mesoscale, the fine balance of non-neighboring interactions dictates the robustness and transformability of supramolecular architectures, offering a powerful guiding principle for the rational engineering of mechanically adaptive mesoscopic materials.

Conclusions

In conclusion, this work demonstrates that the integration of highly aggregative porphyrin chromophores into a scissor-shaped molecular framework activates curvature-directed assembly pathways that give rise to well-defined mesoscale self-assembled topologies. Open-ended helicoidal assemblies evolve spontaneously into tubular architectures, whereas the application of mechanical perturbation through sonication converts them into close-ended nanorings. These results highlight curvature as a decisive design parameter that bridges molecular geometry and self-assembled topology, offering a general strategy to engineer functional π-conjugated chromophores into precisely curved nanostructures. Ongoing studies are extending this curvature-guided approach to diverse functional chromophores to explore its potential in programmable nano-to-mesoscopic material design.

Author contributions

S. Y. and R. Ka. designed the project. R. Ka. performed all the experimental work. S. Y. and R. Ka. prepared the overall manuscript, including figures. All authors, including S. O., H. H., and R. Ku., contributed by commenting on the manuscript. S. Y. supervised the overall research.

Conflicts of interest

There are no conflicts to declare.

Data availability

The data that support the findings of this work have been included in the main text and supplementary information (SI). Supplementary information is available. See DOI: https://doi.org/10.1039/d5sc09619g.

Acknowledgements

This work was supported by the Japan Society for the Promotion of Science (JSPS) KAKENHI grant no. 22H00331, 23H04873 and 24H01710 in a Grant-in-Aid for Transformative Research Areas "Materials Science of Meso-Hierarchy." The authors thank the Materials Analysis Division, Institute of Science Tokyo for MALDI-TOF-MS analysis.

Notes and references

1 L. Brunsveld, B. J. B. Folmer, E. W. Meijer and R. P. Sijbesma, *Chem. Rev.*, 2001, **101**, 4071–4098.
2 T. Aida, E. W. Meijer and S. I. Stupp, *Science*, 2012, **335**, 813–817.
3 J. P. Hill, W. Jin, A. Kosaka, T. Fukushima, H. Ichihara, T. Shimomura, K. Ito, T. Hashizume, N. Ishii and T. Aida, *Science*, 2004, **304**, 1481–1483.
4 D. D. Prabhu, K. Aratsu, Y. Kitamoto, H. Ouchi, T. Ohba, M. J. Hollamby, N. Shimizu, H. Takagi, R. Haruki, S. Adachi and S. Yagai, *Sci. Adv.*, 2018, **4**, eaat8466.
5 B. Shen and M. Lee, *Polym. Chem.*, 2019, **10**, 6551–6554.
6 H.-X. Wang, X. Zhu and M. Liu, *Chem. Soc. Rev.*, 2025, **54**, 5516–5550.
7 S. Yagai, Y. Kitamoto, S. Datta and B. Adhikari, *Acc. Chem. Res.*, 2019, **52**, 1325–1335.
8 S. Datta, S. Takahashi and S. Yagai, *Acc. Mater. Res.*, 2022, **3**, 259–271.
9 K. Aratsu and S. Yagai, *ChemPlusChem*, 2019, **84**, 619–622.
10 S. Datta, Y. Kato, S. Higashiharaguchi, K. Aratsu, A. Isobe, T. Saito, D. D. Prabhu, Y. Kitamoto, M. J. Hollamby, A. J. Smith, R. Dalgliesh, N. Mahmoudi, L. Pesce, C. Perego, G. M. Pavan and S. Yagai, *Nature*, 2020, **583**, 400–405.
11 K. Tashiro, T. Saito, H. Arima, N. Suda, B. Vedhanarayanan and S. Yagai, *Chem. Rec.*, 2022, **22**, e202100252.
12 F. Würthner, S. Yao and U. Beginn, *Angew. Chem., Int. Ed.*, 2003, **42**, 3247–3250.
13 S. Yao, U. Beginn, T. Gress, M. Lysetska and F. Würthner, *J. Am. Chem. Soc.*, 2004, **126**, 8336–8348.
14 S. Yagai, M. Yamauchi, A. Kobayashi, T. Karatsu, A. Kitamura, T. Ohba and Y. Kikkawa, *J. Am. Chem. Soc.*, 2012, **134**, 18205–18208.
15 J. S. Valera, H. Arima, C. Naranjo, T. Saito, N. Suda, R. Gómez, S. Yagai and L. Sánchez, *Angew. Chem., Int. Ed.*, 2022, **61**, e202114290.
16 T. Saito, T. Kajitani and S. Yagai, *J. Am. Chem. Soc.*, 2023, **145**, 443–454.
17 T. S. Balaban, H. Tamiaki and A. R. Holzwarth, *Top. Curr. Chem.*, 2005, **258**, 1–38.
18 C. M. Drain, A. Varotto and I. Radivojevic, *Chem. Rev.*, 2009, **109**, 1630–1658.
19 H. Lee, H. Park, D. Y. Ryu and W.-D. Jang, *Chem. Soc. Rev.*, 2023, **52**, 1947–1974.
20 K. Venkata Rao, D. Miyajima, A. Nihonyanagi and T. Aida, *Nat. Chem.*, 2017, **9**, 1133–1139.
21 F. Würthner, T. E. Kaiser and C. R. Saha-Möller, *Angew. Chem., Int. Ed.*, 2011, **50**, 3376–3410.
22 R. B. Martin, *Chem. Rev.*, 1996, **96**, 3043–3064.
23 M. M. J. Smulders, M. M. L. Nieuwenhuizen, T. F. A. de Greef, P. van der Schoot, A. P. H. J. Schenning and E. W. Meijer, *Chem. – Eur. J.*, 2010, **16**, 362–367.
24 S. Ogi, K. Sugiyasu, S. Manna, S. Samitsu and M. Takeuchi, *Nat. Chem.*, 2014, **6**, 188–195.
25 B. Shen, Y. Zhu, Y. Kim, X. Zhou, H. Sun, Z. Lu and M. Lee, *Nat. Commun.*, 2019, **10**, 1080.
26 R. Kudo, R. Kawai, S. Takamiya, S. Datta, H. Hanayama, N. Hara, H. Tamiaki and S. Yagai, *Chem. Commun.*, 2025, **61**, 8427–8430.
27 T. Yamaguchi, N. Ishii, K. Tashiro and T. Aida, *J. Am. Chem. Soc.*, 2003, **125**, 13934–13935.
28 C. Oliveras-González, F. Di Meo, A. González-Campo, D. Beljonne, P. Norman, M. Simón-Sorbed, M. Linares and D. B. Amabilino, *J. Am. Chem. Soc.*, 2015, **137**, 15795–15808.
29 B. Gole, V. Stepanenko, S. Rager, M. Grüne, D. D. Medina, T. Bein, F. Würthner and F. Beuerle, *Angew. Chem., Int. Ed.*, 2018, **57**, 846–850.
30 Z. Huang, S.-K. Kang, M. Banno, T. Yamaguchi, D. Lee, C. Seok, E. Yashima and M. Lee, *Science*, 2012, **337**, 1521–1526.
31 R. Oda, F. Artzner, M. Laguerre and I. Huc, *J. Am. Chem. Soc.*, 2008, **130**, 14705–14712.
32 D. Zhao and J. S. Moore, *Org. Biomol. Chem.*, 2003, **1**, 3471–3491.
33 K. Aratsu, R. Takeya, B. R. Pauw, M. J. Hollamby, Y. Kitamoto, N. Shimizu, H. Takagi, R. Haruki, S. Adachi and S. Yagai, *Nat. Commun.*, 2020, **11**, 1623.
34 H. Hanayama, I. Tajima, S. Yamashita, T. Aizawa and S. Yagai, *J. Am. Chem. Soc.*, 2025, **147**, 42330–42341.
35 P. Iavicoli, H. Xu, L. N. Feldborg, M. Linares, M. Paradinas, S. Stafström, C. Ocal, B. Nieto-Ortega, J. Casado, J. T. López Navarrete, R. Lazzaroni, S. De Feyter and D. B. Amabilino, *J. Am. Chem. Soc.*, 2010, **132**, 9350–9362.
36 T. Fukui, S. Kawai, S. Fujinuma, Y. Matsushita, T. Yasuda, T. Sakurai, S. Seki, M. Takeuchi and K. Sugiyasu, *Nat. Chem.*, 2017, **9**, 493–499.
37 N. J. Van Zee, B. Adelizzi, M. F. J. Mabesoone, X. Meng, A. Aloi, R. H. Zha, M. Lutz, I. A. W. Filot, A. R. A. Palmans and E. W. Meijer, *Nature*, 2018, **558**, 100–103.
38 T. Schnitzer, M. D. Preuss, J. van Basten, S. M. C. Schoenmakers, A. J. H. Spiering, G. Vantomme and E. W. Meijer, *Angew. Chem., Int. Ed.*, 2022, **61**, e202206738.
39 P. Jonkheijm, P. van der Schoot, A. P. H. J. Schenning and E. W. Meijer, *Science*, 2006, **313**, 80–83.
40 R. Takahashi and Y. Kobuke, *J. Am. Chem. Soc.*, 2003, **125**, 2372–2373.
41 A. Satake and Y. Kobuke, *Org. Biomol. Chem.*, 2007, **5**, 1679–1691.
42 X. Peng, N. Aratani, A. Takagi, T. Matsumoto, T. Kawai, I.-W. Hwang, T. K. Ahn, D. Kim and A. Osuka, *J. Am. Chem. Soc.*, 2004, **126**, 4468–4469.

43 T. Hori, N. Aratani, A. Takagi, T. Matsumoto, T. Kawai, M. Yoon, Z. S. Yoon, S. Cho, D. Kim and A. Osuka, *Chem. – Eur. J.*, 2006, **12**, 1319–1327.
44 P. Motloch, P. S. Bols, H. L. Anderson and C. A. Hunter, *Chem. Sci.*, 2021, **12**, 1427–1432.
45 M. Rickhaus, M. Jirasek, L. Tejerina, H. Gotfredsen, M. D. Peeks, R. Haver, H.-W. Jiang, T. D. W. Claridge and H. L. Anderson, *Nat. Chem.*, 2020, **12**, 236–241.
46 S. A. L. Rousseaux, J. Q. Gong, R. Haver, B. Odell, T. D. W. Claridge, L. M. Herz and H. L. Anderson, *J. Am. Chem. Soc.*, 2015, **137**, 12713–12718.
47 N. Sasaki, M. F. J. Mabesoone, J. Kikkawa, T. Fukui, N. Shioya, T. Shimoaka, T. Hasegawa, H. Takagi, R. Haruki, N. Shimizu, S. Adachi, E. W. Meijer, M. Takeuchi and K. Sugiyasu, *Nat. Commun.*, 2020, **11**, 3578.